A Two Dimensional Discrete Vortex Method for Bridge Aerodynamics Applications

Allan Larsen[1] and **Jens H Walther**[2]

Abstract. The present paper outlines the basic equations and the salient features of DVMFLOW, a 2D numerical Lagrangian CFD code developed for bluff body applications. Application of DVMFLOW to aerodynamic analyses of two long span bridges is discussed.

1 INTRODUCTION

Slender long span bridges are often found to be flexible and thus sensitive to the action of wind. Aerodynamic considerations thus becomes an important element in bridge design, construction and operation. Aerodynamic investigations of long span bridges have traditionally relied on model-scale experiments carried out in wind tunnels.

Theoretical structural analysis was developed into a practical tool in bridge design during the 1980'ies with the development and sophistication of computer based Finite Element Methods (FEM). Theoretical analysis of flow / structure interaction desirable in bridge engineering have not seen similar development and aerodynamic assessment of bridges is still relying on physical testing of scale models. Present day developments in computer sciences have, however, made computational fluid dynamics (CFD) analysis tools accessible to the bridge designer.

2 BRIDGE AERODYNAMICS

The main structural element in any bridge is the girder which carries the roadway / railway and traffic. The bridge girder is supported by other structural elements such as piers or tower/cable systems, but it is a matter of experience that the girder sustains most of the actions of the wind and thus is responsible for the over-all aerodynamic performance of the bridge.

Due to the large span length to girder width / depth of most bridges, the flow about individual girder cross sections may, in a first approximation, be considered two dimensional. The 2D assumption reduces CFD analysis to characteristic cross sections situated in planes perpendicular to the span. The over all aerodynamic action on the bridge girder is then obtained by combining cross sectional loads assuming strip theory to be valid. The 2D assumption is often evoked in wind tunnel testing of bridges, in support of the popular section model testing technique.

2.1 Choice of methodology

In order to be practical, a 2D bridge aerodynamics code must fulfil the following requirements:

- Be applicable to external flows, i.e. satisfy the "free field" boundary condition at infinity.
- Be applicable to flow about "bluff" cross sections as practical bridge girder cross sections often are build as sharp edged polygons.
- Allow for simulation of flows about moving boundaries as problems related to aeroelastic stability and vortex shedding involves cross sections in oscillatory motion.
- Allow for easy modelling of cross sections and structural dynamic characteristics.

A survey of CFD methodologies available for computer based simulations of fluid flow revealed that the discrete vortex method (see [1], [2]) would fulfil the above requirements.

[1]COWI Consulting Engineers and Planners, DK-2800, Lyngby, Denmark.

[2]Institute of Fluid Dynamics, ETH, Zürich, Switzerland. On leave from Danish Maritime Institute, Lyngby, Denmark

3 BASIC GOVERNING EQUATIONS

The kinematics of an incompressible fluid having kinematic viscosity ν and density ρ flowing in a two dimensional domain F about a body B is governed by the Naviér-Stokes equations:

$$\frac{\partial \vec{u}}{\partial t} + \left(\vec{u}\cdot\vec{\nabla}\right)\vec{u} = -\frac{1}{\rho}\vec{\nabla}p + \nu\vec{\nabla}^2\vec{u} \quad \text{in } F \tag{1}$$

$$\vec{\nabla}\cdot\vec{u} = 0 \quad \text{in } F \tag{2}$$

$$\vec{u} = \vec{u}_B \quad \text{on } B \tag{3}$$

the dependent variables being the velocity vector $\vec{u}$ and pressure p. $\vec{u}_B$ is the surface velocity of B.

Equations (1) and (2) constitute the equations solved in traditional computational fluid dynamics codes. The solution procedure taken is to subdivide F in a computational mesh and then solve (1) and (2) in a finite difference or finite element formulation. In doing so, it becomes necessary to design a computational mesh which is dense in regions close to B where large velocity gradients are expected to develop (in boundary layers and wakes) and less dense away from B. The mesh generation process is often tedious and may have a direct influence on the accuracy of the results.

3.1 Vorticity formulation

Taking the curl of (1) recasts the 2D Naviér-Stokes equations into a "transport equation" for vorticity, $\vec{\omega} = \omega\vec{e}$ which in 2D may be considered a scalar quantity ($\vec{e}$ is the unit vector normal to F):

$$\frac{\partial \omega}{\partial t} + \left(\vec{u}\cdot\vec{\nabla}\right)\omega = \nu\vec{\nabla}^2\omega \tag{4}$$

Equation (4) may be split into an advection part (Euler's equation) and a diffusive part (diffusion equaton):

$$\frac{\partial \omega}{\partial t} + \left(\vec{u}\cdot\vec{\nabla}\right)\omega = 0 \tag{5}$$

$$\frac{\partial \omega}{\partial t} = \nu\vec{\nabla}^2\omega \tag{6}$$

The velocity $\vec{u}$ is related to the vorticity ω by the Cauchy Riemann equations $\vec{\omega} = \vec{\nabla}\times\vec{u}$, $\vec{\nabla}\cdot\vec{u} = 0$ or by Biot-Savart relation:

$$u(\vec{x},t) = \vec{U} - \frac{1}{2\pi}\int_F \frac{\vec{\omega}_0\times(\vec{x}_0-\vec{x})}{|\vec{x}_0-\vec{x}|^2}d\vec{x}$$

$$+\frac{1}{2\pi}\oint_B \frac{(\vec{x}_0\cdot\vec{n})\cdot(\vec{x}_0-\vec{x}) - (\vec{u}_0\times\vec{n})\times(\vec{x}_0-\vec{x})}{|\vec{x}_0-\vec{x}|^2}d\vec{x} \tag{7}$$

where $\vec{U}$ is the irrotational onset flow velocity, $|\vec{x}_0-\vec{x}|$ is the distance from a patch of vorticity $\vec{\omega}_0 = \omega_0\vec{e}$ located at $\vec{x}_0$ to a field point $\vec{x}$. $\vec{n}$ is the unit vector normal to B.

The vorticity at the body surface is obtained via the Biot-Savart relation (7) in which the value of the integrals over F and B are known, except for the contribution from the surface vorticity. Introducing a surface vortex sheet γ defined by:

$$\frac{\partial \gamma}{\partial \vec{n}} = \omega \tag{8}$$

allows the unknown surface vortex sheet γ to be defined by a Fredholm type integral equation:

$$\int_B \frac{\vec{\gamma}_0\times(\vec{x}_0-\vec{x}_B)}{|\vec{x}_0-\vec{x}_B|^2}d\vec{x}_B = I(\vec{x}_B) + 2\pi\left(\vec{U} - \vec{u}(\vec{x}_B)\right) \tag{9}$$

where $|\vec{x}_0-\vec{x}_B|$ is the distance from a vortex patch $\vec{\gamma}_0$ situated at $\vec{x}_0$ on B to another point $\vec{x}_B$ located on the contour of B. The vector $I(\vec{x}_B)$ represents the induced velocity from the vorticity in the fluid. The solution of (9) in the unknown $\vec{\gamma}_0$ is unique up to a constant, i.e. an infinite number of solutions exist.

The solution is made unique by evoking the Kelvin circulation theorem which states that the rate of change of the total vorticity in both the body B and the fluid F is zero:

$$\frac{\partial}{\partial t}\int_{F+B}\omega\, d(F+B) = 0 \tag{10}$$

Thus if the total vorticity is zero at $t = 0$ it remains zero for $t > 0$.

4 DISCRETE VORTEX METHOD

The vorticity formulation of the flow equations is solved by taking a Lagrangian or particle approach progressing in time. The solution procedure follows five major actions within each step in time:

1. Determination of the surface vortex sheet $\gamma(\vec{x}_B)$ on B to satisfy the no penetration boundary condition .
2. Diffusion of vortex sheets by transformation of the sheets into vortex "blobs" or particles of strength Γ_p and subsequently diffusing them into the flow by random walks.
3. Advection of discrete vortex particles allowing for mutual interaction.
4. Diffusion of vortex particles allowing for the effect of viscosity.
5. Computation of aerodynamic pressure and forces acting on B.

4.1 Surface vortex distribution

The vortex distribution on B is obtained by subdividing the contour of B into M line segments assuming a spatial linear variation of $\bar{\gamma}_0$ along each "panel". Equation (9) is then approximated by a set of $M+1$ linear equations:

$$\overline{\overline{A}} \cdot \vec{\gamma} = \vec{b} \tag{11}$$

where the matrix $\overline{\overline{A}}$ contains the induced normal velocity component at the i'th panel from the j'th panel as well as the individual panel lengths.

The right hand side vector $\vec{b}$ contains the induced normal velocity at the i'th panel from the vortices in the flow and the total vorticity in the system. The latter is required to render the solution unique in accordance with Kelvin's theorem. The detailed structure of (12) is somewhat involved, but can be found in standard text books on potential flow panel methods (see [3]). The system of linear equations is solved in the least squares sense.

The specific vortex distribution determined from (12) is then assigned to nascent vortices which are placed on B. Nascent vortices are diffused into the flow applying a one-sided random walk method which satisfies (6). A Gaussian probability density function is applied:

$$P(w) = \frac{1}{\sqrt{\pi \nu \delta t}} \exp\left(\frac{-w^2}{4\nu\delta t}\right) \tag{12}$$

where $w > 0$ and δt is the time step length.

Once introduced in the flow, the individual vortex particles are assigned a radially symmetric Gaussian strength distribution. The strength of each particle is then assumed to remain invariant throughout the remainder of the simulation. Individual vortex particles diffused into the flow then form a compound vorticity field of the form:

$$\omega(\vec{x},t) = \sum_p^N \Gamma_p \frac{1}{2\pi\sigma^2} \exp\left(-\frac{\left(\vec{x} - \vec{x}_p(t)\right)^2}{2\sigma^2}\right) \tag{13}$$

where σ is a vortex core radius, with N being the total number of vortex particles in the flow.

4.2 Vortex advection and diffusion

The Lagrangian solution to (5) and (6) involves tracking of vortex particles $(\vec{x}_p, \Gamma_p)$ according to the following ordinary differential equations

$$\frac{d\vec{x}_p}{dt} = \vec{u}(\vec{x}_p, t) \tag{14}$$

$$\frac{d\omega}{dt} = \nu \vec{\nabla}^2 \omega \tag{15}$$

An equation for tracking of vortex positions $\vec{x}$ in F is obtained by combining (5) and (14):

$$\frac{d\vec{x}_p}{dt} = \vec{U} - \sum_{q=1, p\neq q}^{N} \left(1 - \exp\left(-\frac{\Delta_{pq}^2}{\sigma^2}\right)\right) \frac{\hat{\Delta}_{pq}\Gamma_p}{2\pi\Delta_{pq}^2} \tag{16}$$

where $\Delta_{pq} = \vec{x}_p - \vec{x}_q$, the distance between vortex particles p and q.

Equation (16) is solved numerically by ordinary differential equation methods. The diffusion equation (16) is again approximated by random walks to

simulate the effect of viscosity. The combined solution to (15) and (16) using Euler integration is:

$$\vec{x}_p^{k+1} = \vec{x}_p^k + \vec{u}\left(\vec{x}_p^k\right)\delta t + \vec{\eta}_p \qquad (17)$$

where $\vec{x}_p^k$ is the position of the p'th vortex particle at the k'th time step, and $\vec{\eta}_p$ is a random number with zero mean and variance $2\nu\delta t$.

4.3 Aerodynamic forces

The main objective of flow simulations in bridge aerodynamics is to obtain time traces of the aerodynamic forces acting on B. In the case of bluff bodies the major contribution to the forces originate from the pressure distribution. Only an insignificant fraction may be ascribed to fluid shear stress along the surface. Observing the no-slip boundary condition $\vec{u} = \vec{u}_B$, the Naviér-Stokes equations reduces to:

$$\frac{1}{\rho}\frac{\partial p}{\partial \vec{s}} = -\nu\frac{\partial \omega}{\partial \vec{n}} - a_s \qquad (18)$$

where a_s is the tangential acceleration of the boundary and $\vec{n}$, $\vec{s}$ are the unit normal and tangential vectors to B. Neglecting now the stream wise diffusion at B the vorticity transport equation (4) reads:

$$\frac{\partial \omega}{\partial t} = \nu\frac{\partial^2 \omega}{\partial \vec{n}^2} \qquad (19)$$

which, in combined with (8) yields:

$$\frac{1}{\rho}\frac{\partial p}{\partial \vec{s}} = -\frac{\partial \gamma}{\partial t} - a_s \qquad (20)$$

The flux of the circulation of the i'th boundary panel of B is given by:

$$\left(\frac{\partial \gamma}{\partial t}\right)_i = \frac{\gamma_i^{k+1} - \gamma_i^k}{\delta t} \qquad (21)$$

Equation (21) is thus integrated using the discrete circulation flux (23) along the solid boundary:

$$\frac{1}{\rho}\oint_B \frac{\partial p}{\partial s} = -\sum_i \frac{\gamma_i^{k+1} - \gamma_i^k}{\delta t}\Delta s_i - 2S\frac{\Omega^{k+1} - \Omega^k}{\delta t} \qquad (22)$$

where S is the body surface area and Ω^k is the body angular velocity at time step k.

5 NUMERICAL IMPLEMENTATION

Observation of (17) indicates that a "naive" solution involves a large number of arithmetic unit operations per time step, proportional to the number of vortices squared $O(N^2)$, and have proven prohibitive for practical applications involving N = 30.000 - 60.000 vortices. This computational problem is overcome by adapting the fast multipole algorithm (see [4]) which reduced the number of unit operations to $O(N)$.

Also to limit the number of computational operations, vortices in the body wake are pooled when sufficiently far downstream of the body, here $|\vec{x}_p| > 6$. Two vortices are pooled provided they satisfy the following relation:

$$\left|\frac{\Gamma_p\Gamma_q}{\Gamma_p + \Gamma_q}\right|\left|\vec{x}_p - x_q\right|^2 < \varepsilon \qquad (23)$$

where ε is a small number.

6 PRE AND POST PROCESSING

The input to DVMFLOW simulations is a vortex panel model of the cross section to be analysed, i.e. a polygon of typically 200 - 400 line segments which approximates the external contour of the section shape under consideration. The cross section may be fixed in space for determination of mean wind load coefficients, driven in prescribed cross-wind or rotational oscillatory motion for determination of flutter coefficients. Finally the cross section may be assigned a body mass and supported by a linear spring stiffness for simulation of flow induced oscillations.

The output of DVMFLOW are time series of aerodynamic section loads (lift, drag and moment) and section motions. In addition maps of pressure distributions, streamlines and vortex positions at prescribed time steps are available.

Post processing routines are available for determination of mean lift, drag and moment coefficients (C_d, C_l, C_m) as well as aerodynamic derivatives ($H^*_{1..4}$, $A^*_{1..4}$) following the notation introduced by Simiu and Scanlan.

7 APPLICATIONS

DVMFLOW has been tested for analysis of a number of bluff body flows for which wind tunnel model test results and analytical approximations are available. Reference [5] discusses the simulation of flow past a flat plate, stationary in space and in forced vertical and rotational motion. In [6] the application of DVMFLOW to aerodynamic analysis of typical bridge girder cross sections are discussed and comparison to wind tunnel test results is presented. Both references establishes satisfactory agreement between simulations and analytical / experimental results. In the following sections the application of DVMFLOW to analysis of long span bridges is illustrated through two examples involving suspension bridges.

7.1 Great Belt East Bridge

The Great Belt East Bridge situated in Denmark, Figure 1, was completed and opened to traffic early June 1998.

Figure 1. Great belt East Bridge displaying the configuration of the suspended spans and the approach bridges.

The structure comprises a 1624 m main span suspension bridge flanked by approach bridges designed as continuos beams supported by piers. The girders of the main bridge as well as the approaches are designed as closed steel box girders of trapezoidal cross section. The record span for this type of structure warranted elaborate wind tunnel testing for determination of girder cross section shapes and assessment of aerodynamic performance. These results (see [7]) will serve as basis for comparison with simulated data.

7.1.1 Drag coefficients, suspension bridge

The drag loading on a bridge girder constitutes the most prominent horizontal loading component on a bridge structure. The along wind drag coefficient C_d thus becomes the primary target for computer simulations.

The C_d simulations presented below were carried out using stationary panel models of the final girder cross section adopted in the design of the suspension bridge. The H9.1 panel model reproduced the basic trapezoidal shape of the cross section but omitted the light hand rails and the median divider included in the wind tunnel model. The H9.2 cross section featured the same trapezoidal shape as H9.1 but included panel models of the four horizontal slats of rectangular cross section forming 3.5 m high wind screens of 50% porosity added to the basic cross section shape. Stationary simulations of the flow about H9.1 and H9.2 were run for 30 non-dimensional time units $t = TU / B$ where T is time, U is wind speed and B now is cross section width. A non-dimensional time increment $\delta t = 0.025$ and a Reynolds Number $R = 10^5$ was adopted for all simulations discussed.

The desired C_d was obtained from the simulations as the mean value of the C_d traces. Figure 2 displays the first 10 non-dimensional time units obtained for H9.1 and H9.2.

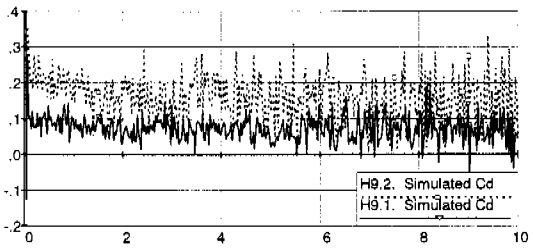

Figure 2. Simulated time traces of C_d for the H9.1 (full) and H9.2 (dot) cross section.

Initially very high C_d values are found due to the abrupt onset of the flow. After approximately 2 non-dimensional time units, the simulated C_d traces settles to fluctuate about mean values of C_d = 0.07 for the H9.1 section and C_d = 0.15 for the H9.2 section. Wind tunnel tests [7] yields C_d = 0.08 and C_d = 0.17 respectively. Visualisation of the simulated flow fields obtained by plotting of instant velocity vectors at an instant in time, here t = 10, are sown in Figure 3. It is noted that the presence of the wind screens leads to a widening of the wake which is consistent with the increase in C_d.

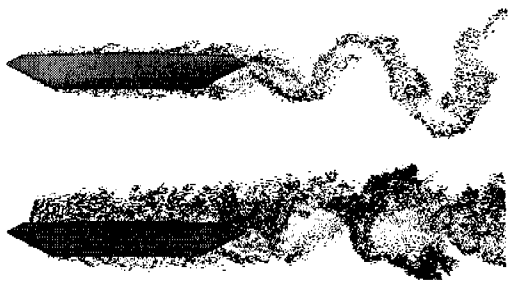

Figure 3. Simulated flow fields about the H9.1 (top) and H9.2 (bottom) cross sections.

7.1.2 Flutter simulation, suspension bridge

The critical wind speed U_c for onset of 2DOF aeroelastic stability (or binary flutter) of the H9.1 cross section was investigated in [6]. Aerodynamic derivatives were obtained from DVMFLOW simulations of flow about the H9.1 cross section driven in sinusoidal rotary and translatory vertical motion at non-dimensional wind speeds ranging from 4 to 16. Good agreement was established between simulations giving U_c = 73 m/s and the wind tunnel tests which yielded U_c = 70 - 75 m/s.

An alternative approach to the traditional flutter analysis based on aerodynamic derivatives, involves simulation of the flow about a 2DOF elastically supported panel model at increasing onset flow speeds. In order to be representative of the prototype, the panel model must be assigned identical non-dimensional rotary inertia $I/\rho B^4$ and translatory inertia $m/\rho B^2$, where I is the cross section mass moment of inertia / unit length and m is the cross section mass / unit length. The rotary and translatory spring constants of the elastic supports are adjusted the reflect the reduced wind speeds $U/f_\alpha B$ and $U/f_h B$ of the simulation:

$$c_\alpha = \left(2\pi \frac{f_\alpha B}{U}\right)^2 \frac{I}{\rho B^4}\,,\; c_h = \left(2\pi \frac{f_h B}{U}\right)^2 \frac{m}{\rho B^2}$$

where f_α , f_h are the eigenfrequencies of the bridge in the torsion and vertical bending modes which are likely to couple in 2DOF flutter. Similar scaling principles are applied in wind tunnel section model testing. The structural dynamics properties of the H9.1 cross section are given in Table 1 below.

Table 1.Structural dynamic properties, H9.1 cross section

I kgm^2/m	m kg/m	f_α Hz	f_h Hz	B (m)
$2.47 \cdot 10^6$	$22.74 \cdot 10^3$	0.278	0.100	31.0

Figure 4 and Figure 5 displays simulated time traces of angular rotation (α) and vertical translation (h) of the H9.1 cross section at wind speeds U = 69 m/s and U = 78 m/s respectively.

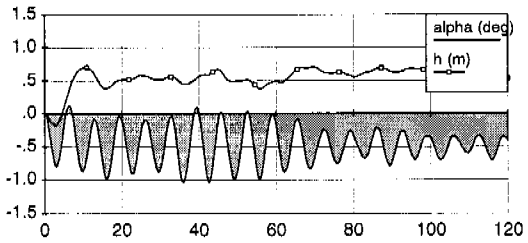

Figure 4. Simulated time traces of angular rotation (α filled) and vertical translation (h line) at U = 69 m/s.

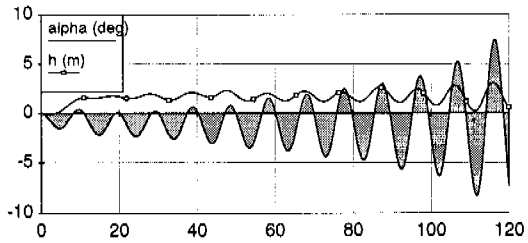

Figure 5. Simulated time traces of angular rotation (α filled) and vertical translation (h line) at U = 78 m/s.

It is noted that the cross section displays small amplitude decaying oscillations consistent with stability at U = 69 m/s. At U = 78 m/s the exponentially growing oscillations of the α and h traces at identical frequency are typical of 2DOF flutter instability. Note the different scale of the vertical axes in Figures 4 and 5.

7.1.3 Vortex excitation, approach bridges

The East Bridge approaches are build as continuos steel girders with 193 m between piers. This span length called for a deep closed trapezoidal box cross section, thus forming a relatively bluff cross section. Vortex induced vertical response was detected in wind tunnel testing as well as for the prototype bridge during erection.

DVMFLOW simulations of the flow induced response of an elastically suspended panel model of the approach bridge cross section, assigned correct non-dimensional mass $m/\rho B^2$ = 21, is shown in Figure 6. The time trace of simulated vertical section motion displays a distinct sinusoidal behaviour characteristic of vortex shedding excitation when the suspension stiffness is tuned to match the frequency of the oscillatory lift.

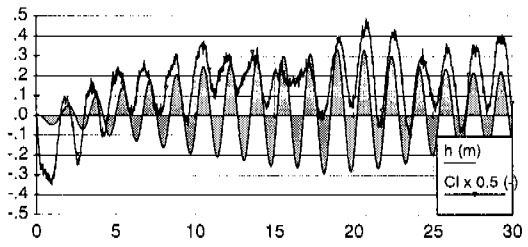

Figure 6. Time traces of simulated vertical response h (filled) and lift coefficient C_l (line).

The simulated lift amplitude h = 0.3 m is in fair agreement with wind tunnel tests ranging from h = 0.3 m - 0.5 m depending on structural damping. Full scale observations of vortex shedding excitation during early construction phases indicated h = 0.2 m. The reduced frequency of the response, based on section depth H, is $f_h H/U$ = 0.17 in good agreement with expected Strouhal Numbers for sharp edged bluff sections. An instant "snapshot" of the simulated flow field, Figure 7 reveals a pronounced menandering wake associated with von Kármán type vortex shedding.

Figure 7. Simulated flow about the East Bridge approach cross section displaying a strongly menandering wake.

7.2 Tacoma Narrows Bridge

The Tacoma Narrows Bridge collapsed in November 1940 in a gale wind speeds of 19 - 20 m/s. The collapse was preceded by approximately an hour of violent twisting motion of the bridge deck, reaching amplitudes of 30 - 35 deg., Figure 8.

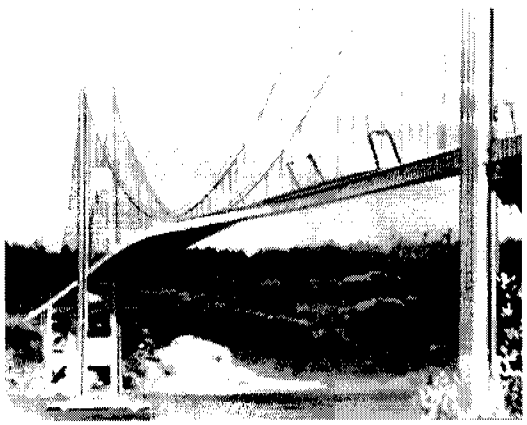

Figure 8. The Tacoma Narrows Bridge twisting under the action of wind during the early phases of collapse.

In the wind tunnel investigation following the collapse, von Kármán and Dunn attributed the violent aerodynamic action to vortices shed at the upwind vertical flange of the cross section. von Kármán's explanation of the aerodynamic excitation mechanism responsible for the collapse have been widely disputed, mainly because the reduced frequency corresponding to the conditions at the collapse,

$f_\alpha H/U$ ≈ 0.66, is 3 - 4 times the value normally associated with vortex shedding excitation.

DVMFLOW simulations of a 1DOF elastically suspended panel model of the bridges shallow H-shaped cross section was carried out in for non-dimensional wind speeds $U/f_\alpha B$ ranging from 1 to 6. The cross section was given an initial angular deflection of 10 degrees and was then released to respond freely for 10 periods under the influence of aerodynamic, inertia and damping forces (ζ = 0.005 relative to critical). The objective was to capture aerodynamic forces and twist response of the cross section and relate these quantities to the vortex dynamics.

At high non-dimensional wind speeds (i.e. $U/f_\alpha B$ = 6) the structural motion is slow relative to the vortex formation and drift process. A clockwise leading edge vortex is created while the section is moving toward higher angles α (nose up). As α peaks and starts to descent, the vortex drifts to a position downwind of the elastic axis. As a result the aerodynamic moment leads the motion (Figure 9, top).

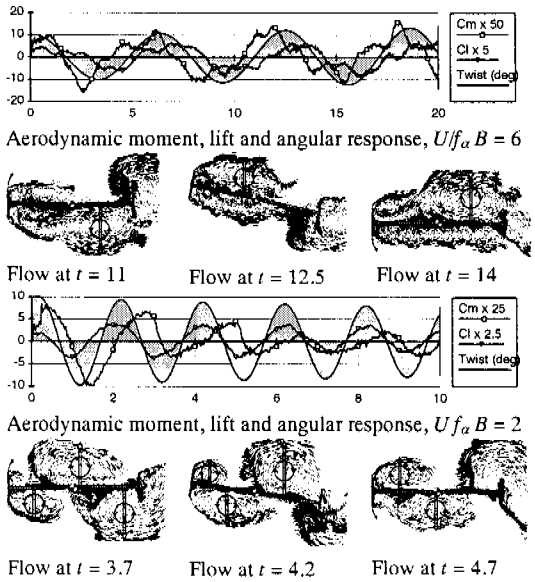

Figure 9. Fee oscillation simulations at $U/f_\alpha B$ = 6 (top) and $U/f_\alpha B$ = 2 (bottom).

At low reduced wind speeds (i.e. $U/f_\alpha B$ = 2) the section response is fast relative to the vortex formation and drift process. The vortex formed at the leading edge during nose up motion will not have sufficient time to develop and drift downwind of the elastic axis before the section motion changes to the nose down direction. The aerodynamic moment will thus counteract the section motion leading to an exponentially decaying twist response (Figure 9, bottom).

The DVMFLOW simulations presented in Figure 9 thus corroborate von Kármán and Dunn's observation that the torsion instability of the H-shaped Tacoma Narrows cross section is driven by vortex formation at the upwind flange of the bridge girder. The vortex formation is thus not linked to the classical vortex street wake depicted in Figure 6.

Having simulated the features of the flow field around the H shaped cross section it is of interest to compare stability predictions based on the simulations the original wind tunnel tests of the Tacoma Narrows Bridge. Figure 10 plots the predicted onset wind speed for the 1DOF torsion instability on the response diagram obtained for a 1:50 scale full aeroelastic model of the bridge. It is noted that the onset wind speed of 3.3 ft/s predicted from the DVMFLOW simulations is in good agreement with the incipient torsion movement recorded in the response diagram.

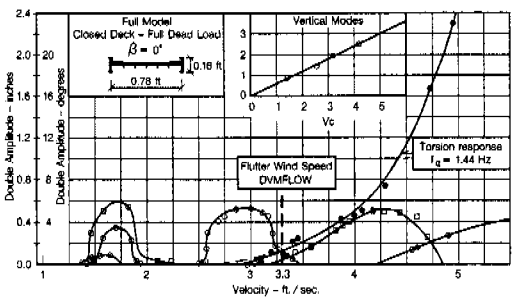

Figure 10. Comparison of onset wind speed for torsion instability (1DOF flutter) obtained from simulations to the torsion response curve (f_α = 1.44 Hz) obtained from wind tunnel tests.

8 CONCLUSION

The present paper has presented the basic considerations and governing equations for the two dimensional Lagrangian CFD code DVMFLOW. From the examples discussed it is concluded that the discrete vortex method is well suited for simulation of flows about bluff sharp edged cross sections often encountered in design of long span bridges. The bridge designer may now take advantage of CFD for acquisition of aerodyanmic design data and gain understanding of flow structure interactions - certainly faster and probably at less cost than required for wind tunnel testing. As a new design tool, CFD has not yet established a long track record of applications. CFD is thus not viewed as a substitution for all wind tunnel testing. Rather, it is seen as an efficient tool for exploring designs and weeding out inefficient cross sections before selecting promising designs for final experimental verifications.

9 REFERENCES

[1] G. Turkyyah and D. Reed, *Fast vortex methods for wind-induced pressures on buildings*, 51-79. Journal of Wind Engineering and Industrial Aerodynamics, 58, Elsevier Science, 1995.

[2] R. I. Lewis, *Vortex element methods for fluid dynamic analysis of engineering systems. Cambridge University Press*, 1991.

[3] A. M. Kuethe and C. Chow, *Foundation of aerodynamics*, John Wiley and Sons, 1986.

[4] J. Carrier, L. Greengard and V. Rokhlin, *A fast adaptive algorithm for particle simulations*, 669-686. SIAM, Journal of Scientific and Statistical Computation, 9

[5] J. H. Walther and A. Larsen, *Two dimensional discrete vortex method for application to bluff body aerodynamics*, 183-193. Journal of Wind Engineering and Industrial Aerodynamics, 67&68, Elsevier Science, 1997.

[6] A. Larsen and J.H. Walther, *Aeroelastic analysis of bridge girder sections based on discrete vortex simulations*, 253-265. Journal of Wind Engineering and Industrial Aerodynamics, 67&68, Elsevier Science, 1997.

[7] A. Larsen, *Aerodynamic aspects of the final design of the 1624 m suspension bridge across the Great Belt*, 261-265. Journal of Wind Engineering and Industrial Aerodynamics, 48, Elsevier Science, 1993.